Acta Materialia 212 (2021) 116929

Contents lists available at ScienceDirect

Acta Materialia

journal homepage: www.elsevier.com/locate/actamat

Full length article

Revealing Nanoscale deformation mechanisms caused by shear-based material removal on individual grains of a Ni-based superalloy

Dongdong Xu[a,1], Thomas E.J. Edwards[b,1], Zhirong Liao[a], Xavier Maeder[b], Rajaprakash Ramachandramoorthy[b], Manish Jain[b], Johann Michler[b], Dragos Axinte[a,*]

[a] Faculty of Engineering, University of Nottingham, NG7 2RD UK
[b] Empa, Swiss Federal Laboratories for Materials Science and Technology, Laboratory for Mechanics of Materials and Nanostructures, Thun 3603, Switzerland

ARTICLE INFO

Article history:
Received 25 November 2020
Revised 4 April 2021
Accepted 20 April 2021
Available online 27 April 2021

Keywords:
Shear
Nanoscale deformation
Grain boundary
Superalloy
Micromechanics

ABSTRACT

Shear-based material removal processes significantly influence the quality of workpiece surface and implicitly the component functional performance. An *in-situ* SEM nano-cutting enabled the study of crystal flow and lattice rotation occurring below the cutting edge in a polycrystalline Nickel superalloy. When nano-cutting within single grains a deformed nanolayer appears that consists of a crystal lattice rotated exclusively within the cutting plane which is delimited from the bulk of the grain by high angle boundary (HAB); the depth of deformed nanolayer increases with the material pile-up (nano-chip) caused by the grain shearing. Upon nano-cutting multiple grains, nano-recrystallisation at the HAB occurs, accompanied by the bending of the grain boundary (GB) in the cutting direction, a phenomenon that also significantly influences the deformation behaviour of the grains cut after passing the GB. Clarifying these aspects at the nanoscale is crucial for understanding the formation of workpiece surface damage after material removal operations.

1. Introduction

Shear-based material removal processes (e.g. cutting) at macro and micro scales have been studied using basic mechanistic theories [1,2] (e.g. force balancing on homogeneous material) with some recent attempts to link them with plastic deformation of the underlying crystal structures [3,4]. However, the classical mechanistic theories have some difficulties in being applied to micro-machining where the influence of the "secondary" phenomena (e.g. material ploughing) and crystal lattice (e.g. orientation) become of importance in understanding how the process occurs at this scale. This is because, whilst at this scale the micro/nano-mechanics of materials play dominant roles in deformation, the classical shear theory commonly considers the materials as homogeneous and hence, cannot reveal the intricate shear-induced phenomena associated with the process. In particular, the nanoscale shear deformation enforced by tips with defined geometry (clear rake, radius and flank dimension) inside single crystals may not follow the shear-plane theory anymore because of the crystal orientation that influences the preferential slippage behaviour, as well as due to the existence of grain boundaries (GBs) in polycrystals as the small tip size is now comparable to the GB wavelength. It has been noted the existence of GB may cause the sudden change of cutting phenomenon usually causes the formation of a boundary step, which could influence workpiece surface roughness [5]. Thus, when considering cutting at the micro/nano–scale, the governing phenomena that accompany the shear-based process need to be intimately linked with those occurring in each differently oriented grain [6,7], and at grain boundaries [8].

Indeed, crystal texture [9] and defects (e.g. local misorientation, dislocation content) of materials play key roles on determining its properties in various application conditions [10]. It has been essential to study the microstructure variation of materials under different loadings to understand its corresponding responses [11–13]. Small scale uniaxial loading – micro-compression and -tensile testing [14–17] – has been widely used to study crystal deformation. These approaches could represent avenues for open questions on how micro/nano shear-based processes (e.g. cutting) causes material deformation under loading at the grain/grain boundary scale [18]. However, the material deformation in micro/nano cutting (e.g. orthogonal or oblique resulting in 2D or 3D loading) are normally

* Corresponding author.
E-mail address: Dragos.axinte@nottingham.ac.uk (D. Axinte).
[1] Equal contribution from the two authors.

https://doi.org/10.1016/j.actamat.2021.116929

more complex than in uniaxial pillar or simple shear tests as it involves shear loading, friction against the tool faces and ploughing. For example, as a common outcome of micro-cutting, the material is often deformed close to the workpiece surface; however, currently, existing studies stop at the mapping of overall grain plasticity without exploring the mechanisms that the shear induces locally in a single grain and at grain boundaries [19].

Efforts have been made to study grain deformation at micro- and nano-scales by use of scratch tests [20,21]; these have been performed to study the brittle-ductile transition mechanism in brittle materials [21,22] or the deformation response in subsurface areas [23]. These tests might, apparently initially, be considered of relevance to micro/nano-cutting, as they are normally implemented with indenters used for material characterisation (e.g. symmetrical wedge or Berkovich tips). In addition, pure shear deformation in crystals reveals basic deformation properties [24,25]. However, as it will be demonstrated later, these simple loading states are far from the conditions arising upon cutting as the material deformation is difficult to control (inappropriate or inadequate definition of cutting planes due to unadapted tips which lead to poor control of 3D deformations). Furthermore, the low stiffness of the equipment means that even where lateral forces are captured, little correlation between the material deformation and the reaction forces parallel to the scratching direction is possible due to poorly captured rapid deformation bursts, which inhibit deeper understanding of phenomena associated with material deformations along the tip movement direction. Recently, a report on a tribological problem (roller sliding on a surface) was presented where deformation within the grains as well as at the grain boundary has been put in evidence [26]. Nevertheless, by the nature of this loading geometry, the interesting problem stemming from the influence of the material pile-up (i.e. chip formation), caused by the material shearing, upon the deformation of grain and grain-boundary, cannot be studied.

As an alternative to study the material response in cutting phenomena occurring at micro/nano-scales, simulation studies, including molecular dynamics [27–29], atomistic simulations [14,30] and crystal plasticity finite element methods [31,32], have been most popular to study these complex loading conditions [33,34], e.g. nano-cutting [35], from the point of view of dislocation structures [15,27,36], grain refinement [37] and grain size variation [38] in the subsurface regions. Considering the complexity of the cutting problem at the micro/nano-scale, there is no surprise that even these simulations mainly consider monatomic single crystals (e.g. Si, Cu or Al) [27,39,40]. Rarely have simulations been reported for cutting-related deformation in polycrystalline materials [41]. However, no direct observations of the deformation mechanism of grains in complex loading conditions have been reported at sub-micro/nano-scales to elucidate the real occurring phenomena. In this respect, it could be commented that lacking in-depth experimental evidence and understanding of the grain response to the loading resulting from cutting at micro/nano-scales, the inputs in these simulation-based investigations rely on assumptions without considering the complex interaction inside grains, making them, for the time being, more of a speculative nature. Thus, without experimentally studying the phenomena (e.g. dislocation motion, recrystallization, boundary formation etc.) occurring within a grain and its boundaries during material shearing at micro/nano-scales, an in-depth understanding of cutting at these scales will be very challenging.

From the above, it is apparent the importance of carrying out investigations on the mechanisms of deformation of polycrystalline materials in complex loading scenarios. One should consider the evolution of crystalline structures and defect contents at micro/nano-scales, as well as GBs, which are, in fact, of key relevance in determining the surface properties [40,42,43], especially at the micro/nano-scale. To elucidate the cutting-based deformation occurring at the micro/nano-scales, we analyse and explain an unexplored phenomenon within the grain and at the grain boundaries of a polycrystalline engineering material. Using a specifically built, highly stiff, displacement controlled setup, we focus on two dimensional “intra-grain” and “inter-grain” cutting with well-defined nanoscale cutting planes generated by an appropriate tip design (that resembles real shear-based material removal operations). By performing the deformation in vacuo, white layer formation [44] was avoided, such that the intrinsic deformation mechanisms in the near-surface region could be studied without spurious oxygen contamination. We further make use of advanced material characterisation techniques, all to show that the classical mechanistic cutting theory has significant limitations at truly micro/nano-scales. By directly revealing the crystal texture variation of the stress-affected layer from a shear-based material removal scenario, we will fundamentally explain the influence and mechanism of material removal, considering crystal orientation effects, grain boundaries restriction and pile-up material accumulation. Such investigations not only aim to reveal the as-yet unobserved material deformation mechanisms, they will also dramatically feed modelling efforts into small-scale material deformation simulation in complex loading conditions by providing sufficient and direct practical validation and correction.

2. Experimental details

2.1. Experimental setup

To understand the nanoscale deformation mechanism of the single grains and the influence of grain boundaries in polycrystalline materials under a shear-driven material removal process, we employed an *in-situ* cutting method to carry out orthogonal nano-cutting on both single grains and across grain boundaries (Fig. 1) with a specific stock material removal to generate new surfaces (with nano-scale deformed layers), that are the object of our in-depth studies. It is worth noting that the material employed here is not a bi-crystal but a polycrystalline structure which allows to statistically study the nano-cutting of different GBs and orientation grains. In addition, different from the conventional micro/nano-scratching methods, in which only tips for indentation (e.g. *V*-shape or Berkvich ones) are used that makes it difficult to control the removal of the material, the present nano-cutting allows a well-controlled shear of materials and formation of the chips; we also have here full information on 3D cutting forces during SEM *in-situ* cutting.

An Alemnis indenter with a SmarTip tri-axial piezo-electric force measurement device and a continuous movement lateral piezo-electric stage was employed to carry out the nano-cutting tests, while forces in both normal (ND) and cutting (CD) directions were acquired with software from the equipment. The force sensor operates with a 30 μN and 10 μN RMS noise in the ND and CD directions, respectively, and with measurable force ranges of 1 and 0.2 N, respect. A customized diamond (electrically conductive) cutting tip (Fig. 2a) with well-defined geometry (rake angle: 0°; clearance angle: 30°; tip width: 10 μm; and tip radius: 90±5 nm) was employed for the nano-cutting tests. Target grains were located with reference to the fiducial FIB markers and the cutting start position could then be determined. The cutting length was 12 μm; cutting depth was 1 μm and width was 10 μm (determined by the width of the cutting tip). To clarify, these parameters have been used to achieve a low theoretical edge radius vs. chip thickness ratio (smaller than 1/10) that resembles the cutting conditions in real scenarios. In reference to the value of cutting length (12 μm), this has been chosen to enable lift out of lamella for TEM/TKD study. The cutting is carried out as follow: 1) tip pen-

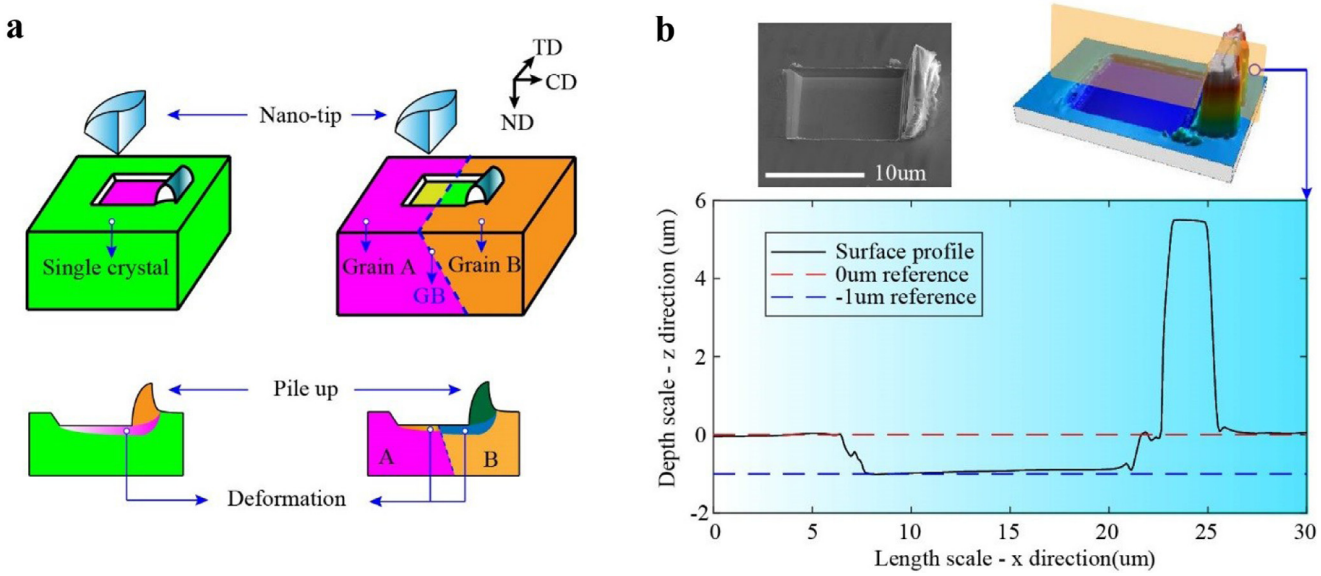

Fig. 1. Overview of nanoscale material removal on a single grain in a polycrystalline material. **a**, Removal of materials on single grain and across a grain boundary to reveal the superficial deformation in both cases. b, SEM view (top left) and the actual geometry of the cut material (constant depth of cut: 1; length: 12; and width 10 μm).

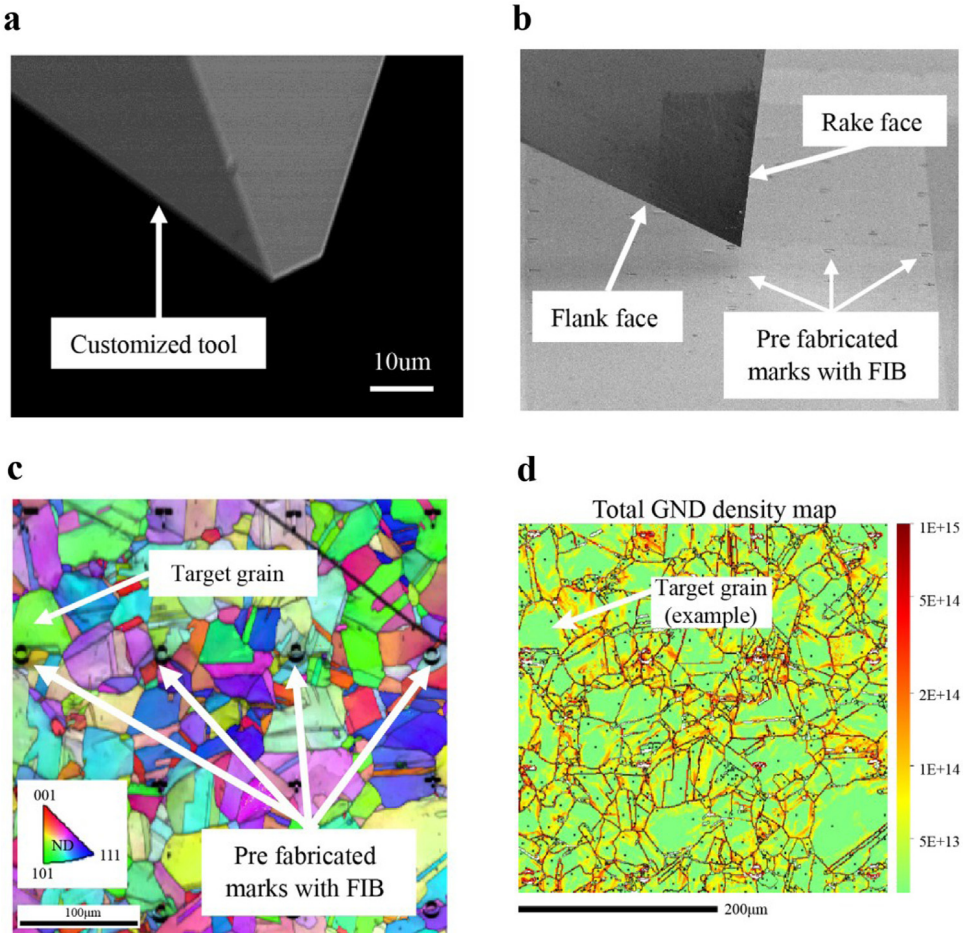

Fig. 2. Overview of the employed cutting tip and investigated sample. a, Diamond nano-cutting edge (90 nm edge radius) employed in this study. **b**, Cutting tip geometry and the relative position with studied sample. Pre-fabricated marks by FIB to locate the relative position of the cutting tip and specific grains in the SEM. **c**, EBSD map before cutting test showing the pre-fabricated marks and individual grain orientation. **d**, Geometrically necessary dislocations (GND) maps to reveal the initial status of the prepared Inconel 718 workpiece. Note: the selected grain for cutting has a relatively low GND density in its bulk.

etrates into the materials to the required (1 μm) cutting depth in perpendicular direction (loading period); 2) tip moves in the cutting direction to the defined cutting length and stops (cutting period); 3) tip retreats in the perpendicular direction to a position above the original worpiece surface (unloading period); and 4) the tip holds in its position to enable the capture of SEM images (holding period). Various cutting conditions were carried out for validation, while only selected examples (tip displacement rate in the loading phase: 0.1 µm/s in ND direction; in the cutting phase: 2 µm/s in CD direction; and in the unloading phase: 0.1 µm/s in ND direction) are presented in current research for detailed discussion. The experiment was carried out in vacuum in a SEM (XL30, FEI, USA) at a constant temperature of 22 °C.

2.2. Materials and sample preparation

A face-centred cubic (FCC) polycrystalline material (Inconel 718 superalloy workpiece with 30 μm average grain size) was used for the micro/nano-cutting tests. The sample was adapted to the size requirements of the nano-indenter machine (Alemnis, Switzerland). After grinding with P400, P800, P1200, and P4000 grit SiC sandpaper (MetPrep, Coventry, UK), the sample was polished gently with 6 and 1 μm diamond suspension and followed by 0.06 μm silica suspension (Buehler, USA). After each preparation step, the specimens were ultrasonically cleaned in isopropanol. The sample was then fixed on an aluminium pin stub with Electrodag (AGG3692, Agar scientific). To enable location of the grain positions on samples when implementing cutting in the scanning electron microscope (SEM), a Ga^+ focused ion beam tool (FEI Quanta200 3D FIB-SEM) was used to make a regular array of marks (cross, circle and T-shape) on the sample surface (Fig. 2b) as reference points. An EBSD map was acquired to identify their position (Fig. 2c) and characterise the initial state of prepared samples (Fig. 2d), using a JEOL7100F scanning electron microscopy (SEM) equipped with an Oxford Instruments AZtec HKL Advanced EBSD System (with NordlysMax3) for crystallographic characterisation.

2.3. Surface topography and superficial microstructure characterisation

The whole cutting process was recorded by video (see supplementary video S1) within the SEM, while the generated surface and shape of chips were captured by post-mortem imaging in the same SEM. Later, the topography of the cut features was accurately measured by 3D optical profiling (Zygo NewView™ NX2 3D Optical Profiler) and processed with MountainsMap (Mountains 7). Post-test EBSD mapping was carried out equivalently to before testing.

Thin lamellae of the nano-cuts for further analysis requiring electron transparency were obtained by a focused ion beam lift out process; a preliminary protection by electron beam-assisted Platinum (Pt) deposition from a metal-organic precursor gas, followed by ion-beam assisted Pt deposition was applied. Transmission electron imaging (TEM) was performed on a JEM2200fs (Jeol, Japan) in bright field scanning (BF-STEM) mode. Transmission Kikuchi diffraction (TKD) was performed with a 30 nm step size (10 nm for high resolution of the near-GB region) on the same thin lamella to generate quantified crystal orientation data from which cutting-induced rotations could be extracted, using an EBSD detector (DigiView 5, TSL/EDAX, USA) mounted on a scanning electron microscope (Mira, Tescan, Czech Republic); data analysis was performed using the OIM Analytics software (TSL/EDAX, USA).

3. Results and discussion

3.1. General results illustration for both single grain and cross-boundary nano-cutting

Initial mapping of crystal orientations (EBSD) was carried out to identify and characterise the target grains where the controlled nano-cutting tests were performed; the initial material state is characterised by a relatively low geometrically necessary dislocation density in the grain interiors, Fig. 2. Following the presented experimental methodology, nano-cutting tests are implemented on both single grains and cross-boundary scenarios (Fig. 1a) to investigate the differential deformation mechanisms between the two site types, and the corresponding generated geometry is measured (measurement of a cut on single grain as example; Fig. 1b). Supplementary Video S1 shows the tip movement and material deformation process during the nano-cutting performed in a scanning electron microscope, while an example of snipped images is presented in the supplementary SE1; the generated surface and the piled-up material (i.e. chips; see Fig. 3) is seen for both single grain and cross-boundary nano-cutting.

3.2. In-Situ *analysis of nano-shear deformation of single grains (Monocrystal)*

EBSD analysis has been employed to reveal the induced misorientation caused by nano-cutting (Fig. 4a) on the single grain (see Fig. 4b). We found clear misorientation (purple colour area in Fig. 4b) on the machined surface compared with the surrounding single crystal (green colour), showing the significant deformation caused by mechanical loads yielded by nano-cutting.

The reaction force on the tip in both normal direction (ND) and cutting direction (CD), and the tip displacement during the cutting process have been monitored (Fig. 5a). Surprisingly, we found that both reaction forces increase as the tip advances in the cutting process along the single grain although the cutting depth remains constant at 1 µm, as seen in the section profile (Fig. 1). This is initially thought to be because the volume of material built-up in front of the cutting tip is increasing as it moves forward (see supplementary SE1), resulting in monotonic increase of friction force between the rake face of the cutting edge and the built-up material. Note that the force drops in the initial moments of cutting because of the releasing contact of the tip flank face with the material, which is explained in the Supplementary Explanation SE2.

To understand the nanoscale material deformation mechanism in the superficial layer generated after shear cutting in a single grain, we lifted out a section of the deformed area in the CD-ND plane (Fig. 5b) using a focused ion beam (FIB) method; transmission Kikuchi diffraction (TKD) crystal orientation mapping was implemented on the acquired sample. No significant crystal rotation was observed about the transverse direction (TD) to the force implementation plane – the cutting plane (see inverse pole figure IPF||TD; Fig. 5c). This suggests that during the cutting process the near-surface material does not plastically deform in the transverse direction (TD), perpendicular to the lift-out section. However, in the IPF||ND and IPF||CD maps (Fig. 5e,f), we observed a significant crystal rotation in the superficial surface region, which may be quantified as misorientation relative to the base material, Fig. 5d. Hence, the near-surface structure of the single grain has been strongly deformed by the nano-cutting, but this only undergoes two-dimensional deformation in the orthogonal loading plane (CD-ND plane), i.e. plane elastoplastic strain. Not only does the force in the cutting direction (CD) increase with increasing volume of pile-up materials (i.e. chips; Supplementary SE1) as the cutting tip advances, Fig. 5a, but this also occurs in correlation with the sub-surface deformed layer penetrating progressively deeper into

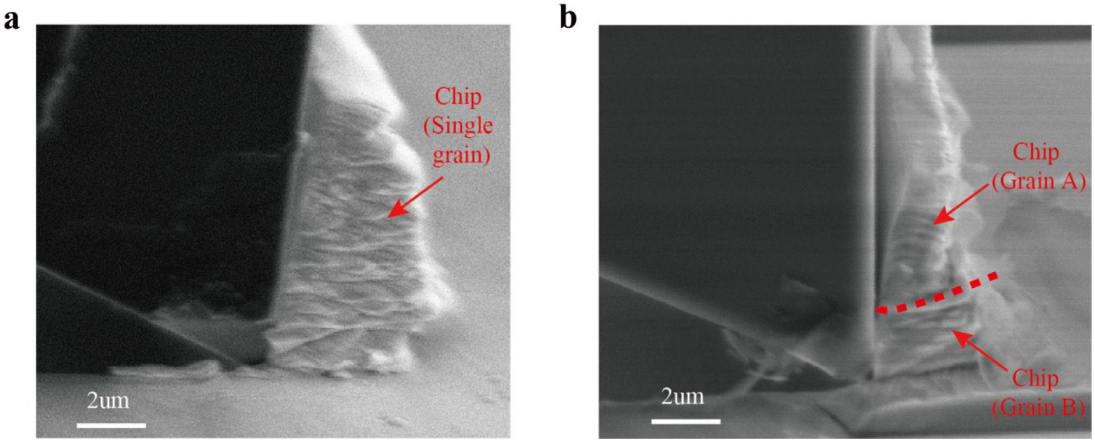

Fig. 3. Generated material pile-up (chips) when nano-cutting a single grain and crossing a grain boundary. a, Uniform (e.g. constant thickness) chip morphology resulting from single grain nano-cutting. **b**, Chip morphology when nano-cutting across a grain boundary shows a clear different chip morphology (e.g. varying thickness) originating from grain A and B; the GB separating the two kinds of chip shapes is indicated by the dashed red line.

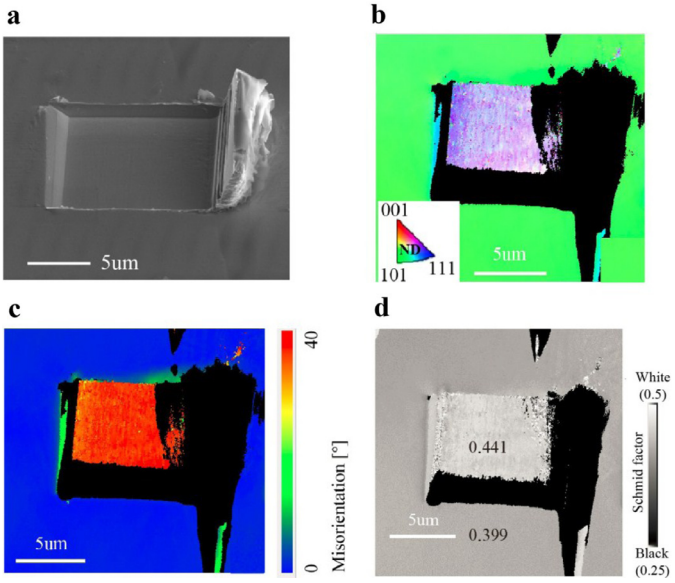

Fig. 4. Enlarged view of crystal orientation (EBSD) and misorientation map on the machined surface of a single grain. a, SEM image of the generated surface after cutting on a single grain. b, EBSD orientation map on single grain after machining. Green colour: the original single grain; General purple colour: the deformed material tends towards similar orientations This was validated with repeated cutting tests on the same grain, revealing the damage introduced from the nano-cutting. Note: the non-indexed regions are because of the shadowing from the generated chips and the side surface of the generated slot which are perpendicular to the EBSD measured surface. c, Misorientation comparison between deformed and undeformed areas after nano-cutting of the single grain. d, The corresponding map of Schmid factor (SF) relative to the cutting direction showing a clear increase (0.399 in bulk to 0.441 in cut area) in the deformed surface.

the substrate material as cutting evolves along the grain. The increase in deformation depth that we prove when nano-cutting a single grain at a constant material removal depth contrasts with the classical macroscopic orthogonal cutting theory, that the generated surface integrity remains stable for a given combination of cutting parameters. It is instead suggested here that the extent of deformation occurring under the cut surface also depends on the material piled-up in front of the tip, a phenomenon that will be shown later has other implications on the grain structural changes.

Further analysis of the nano-texture of the near-surface 2D rotated layer was performed to study the deformation imposed by the cutting of a single grain (Figs. 5,6). We identify high angle boundaries (HAB, misorientation above 15°) between the deformed area and the bulk materials for which there is a local deformation threshold for HAB formation, while crystal rotation-inducing deformation mechanisms, such as slip, are investigated by transmission electron imaging of site-specific lift-outs.

In Fig. 5d, we identify significant bending of the crystal lattice of the grain in the near-surface region, with point-to-point misorientation angles of 2–3°, referred to here as the highly dislocated region - HDR (see the misorientated area in Fig. 4c). At a further depth into the grain, a more significant boundary (misorientation ~15°, i.e. HAB) delimits the HDR from the relatively unreformed (misorientation below 0.5° measurement limit) depth of the bulk, original grain. Therefore, this HAB can be considered as the threshold for crystal rotation (and, more generally, plasticity, as deformation is constrained to the region above this line) upon nano-cutting of a single grain. In addition, in the initial cutting region we found that there is no HAB appearance – misorientations are lower and progressive – indicating that the HAB forms only when a local deformation threshold is reached, Fig. 5d, discussed further below. It is hence the position of this HAB line that is seen to progressively dive into the material depth with increasing cutting force; after a cutting length of 12 μm, no steady-state HAB depth is achieved within a single crystal.

Transmission electron microscopy (TEM) observations (Fig. 6a) confirmed that the as-machined surface layer consisted of inhomogeneous deformation levels along the length of the cut (initial defect accumulation followed by generation of HAB), whilst a shear band at the pile-up base can be straightforwardly identified. As annotated, three areas (I, II, III) at different stages of the cutting process in the single grain are identified. Area I is the start cutting stage (sub-regions R1 and R2 in Fig. 6a) where we do not see a clear boundary between the deformed area and the bulk of the grain, but rather a gradual decrease in dislocation density into the grain depth (detail view in Supplementary Explanation SE3). This corroborates with the gradual misorientation distribution in the same area in Fig. 6b and the absence of the HAB peaks in Fig. 5d. In Area II, a clear horizontal line of high dislocation exists in coincidence with the HAB (Fig. 6a). In the context of sliding wear testing, this feature has been referred to as a DTL [45]: dislocation trace line; however, as we shall see, several interpretations of the tribological DTL differ to our observations in the context of cutting. Below the HAB, a relatively low density of slip traces, along the {111} evidence non-extensive plasticity in the unrotated grain bulk. The deformed region above the HAB shows a more complex array of line defects than the bulk of the grain, which is in line

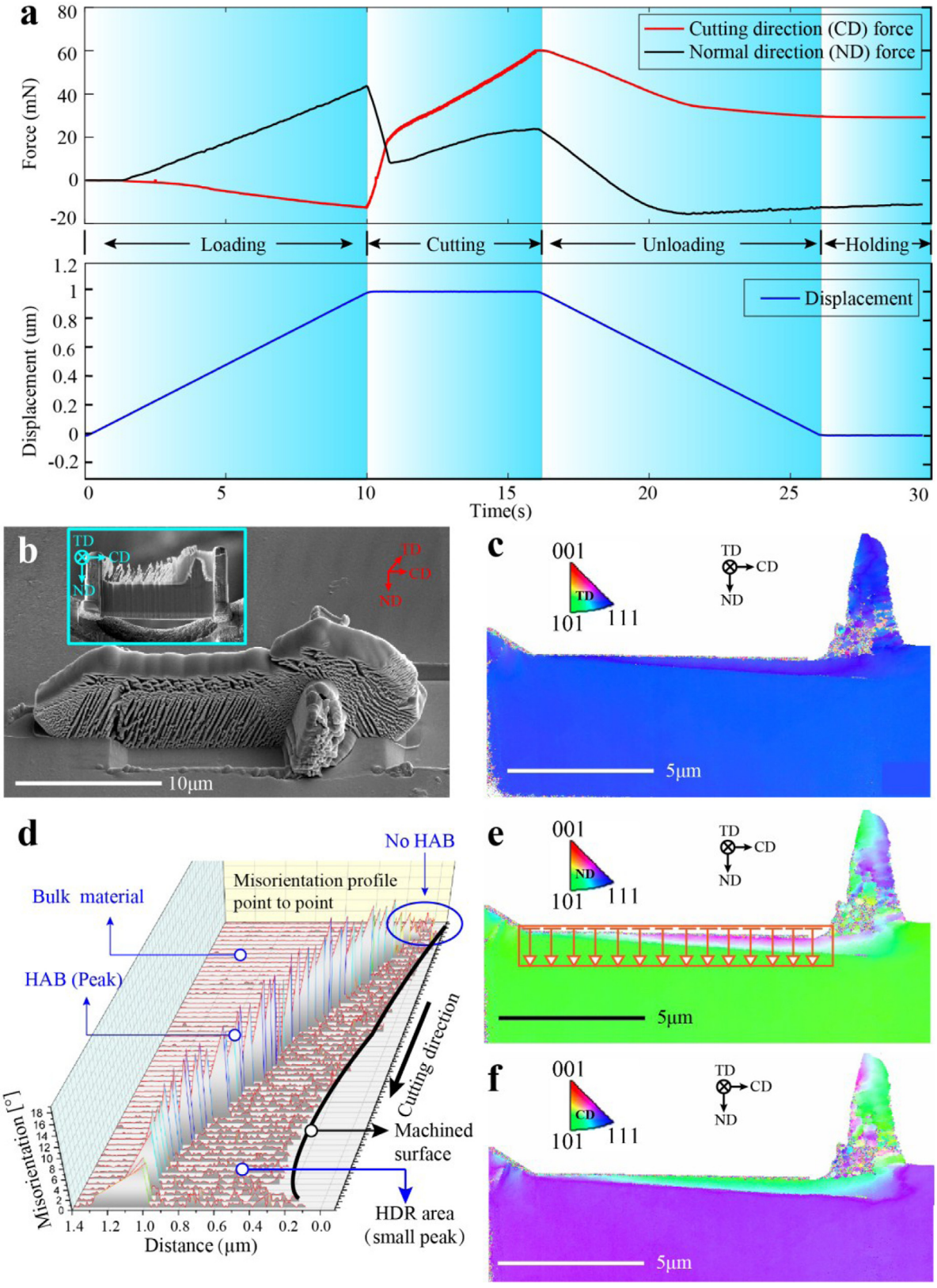

Fig. 5. Crystal orientation in the superficial surface and misorientation distribution in single grain after shear loading. a, Acquired reaction forces in both cutting (CD) and normal (ND) directions in nano-cutting of a single grain along with the displacement of cutting tip. Different stages of the cutting process (i.e. loading, cutting, unloading and holding) are displayed. b, Overview image of the FIB lift-out region and platinum protected area, and as-prepared lamella (inset). (15 × 10 × 100 nm). c, Transmission Kikuchi diffraction (TKD) crystal orientation map with inverse pole figure colouring relative to transverse direction, TD, (IPF||TD). It shows almost the same orientation for the whole subsurface area, indicating that there is almost no lattice rotation relative to TD. d, 3-D view of point-to-point misorientation angle profiles from e of the deformed near-surface region, showing both the highly dislocated region (HDR) and the high angle boundary (HAB). Note that the apparently increasing depth of the machined surface is simply an artefact of the TEM lamella not being perfectly aligned in the TKD holder: a slight in-plane rotation (~1.5°) of the lamella exists; this has no impact on the crystallographic misorientation analyses here; the cutting depth was constant, at 1 μm deep. e, TKD map relative to the normal direction, ND, (IPF||ND) showing the distinct orientation gradient in the near-surface region area, while there is also a gradient in the deformation depth. f. TKD map relative to the cutting direction (IPF||CD).

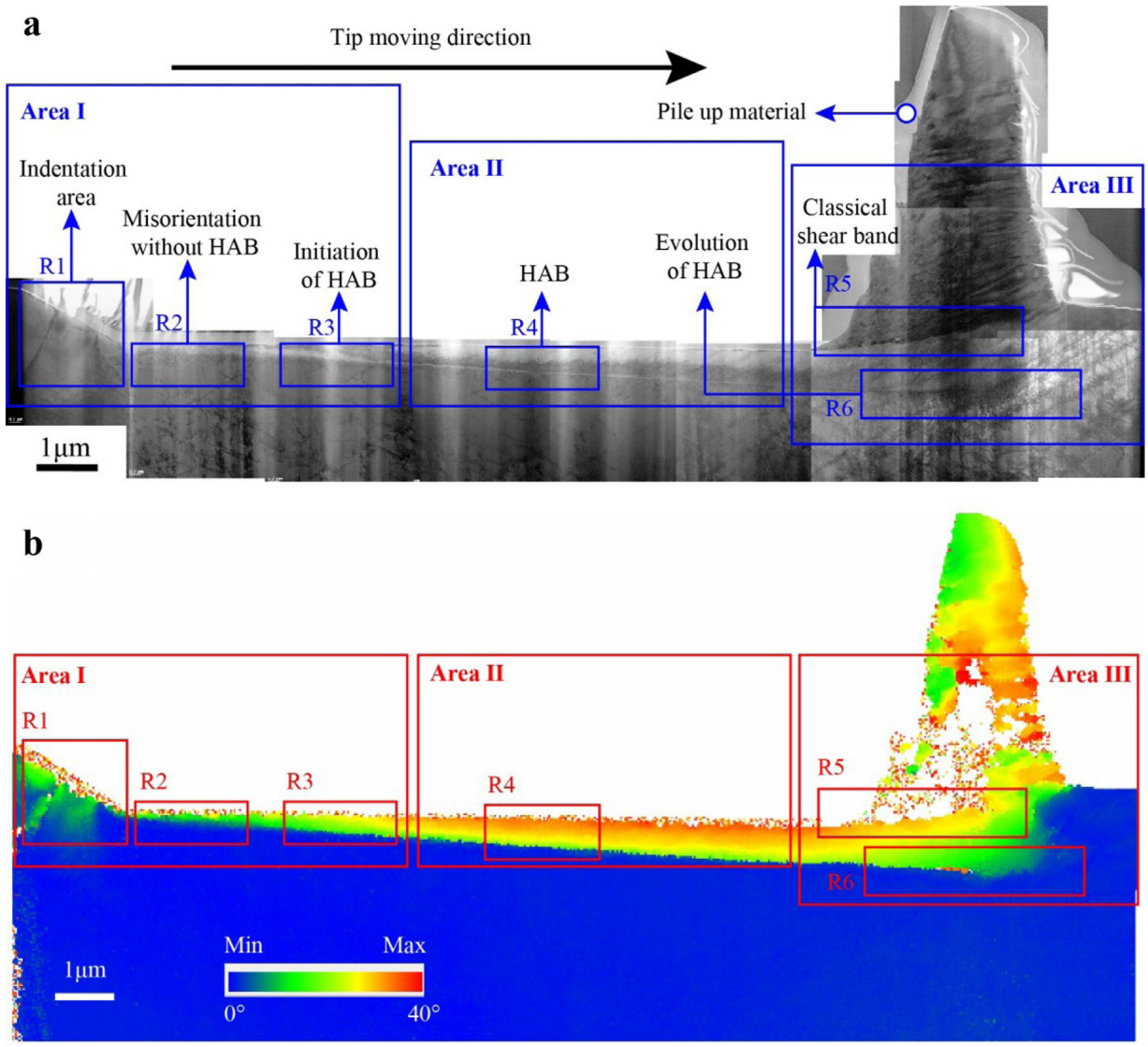

Fig. 6. TEM image and misorientation map reveal the crystal variation structure in sub-surface areas after nano-scale material removal in a single grain. a, Overview bright field scanning TEM image of the whole lift-out lamella showing different deformation mechanism areas. Area I: simple lattice bending and the HAB initiation stage. Area II: the mid-cut part where a steady HAB has been formed. Area III: the deformation of the existing near-surface layer is initiated along with HAB, shear bands and material pile-up (i.e. chip). b, Misorientation map of same area of image a. In Area I, R1 and R2 regions highlight the progressive misorientation caused by initial indentation and cutting without HAB generation, while the HAB starts to appear as a misorientation threshold is achieved in R3 region. In Area II, the misorientation across the HAB is stable (around 15°) with progressive crystal rotation in the HDR from HAB to the free surface of the grain. In Area III, the data reveals the process of material evolving from bulk state to material pile-up (i.e. chip formation) and generated surface. R5 sub-region presents the material pile-up according to the classical shear band mechanism and R6 shows the HAB growth from the bulk material.

with the observed HDR in Fig. 5d as well as the misorientation distribution in Area II in Fig. 6b. A major feature of deformation in this layer is the regularly spaced slip traces, 200–500 nm apart, and angled at ~30° to the cutting direction, i.e. not perfectly parallel to the direction material removal, or to the major shear band at the pile-up base (see later). Finally, Area III presents the scenario of new material being removed, together with near-surface deformation being initiated. The clear shear band (sub-region R5 in Fig. 6) shows that the material pile-up process in a single grain follows the classical orthogonal cutting theory: the material experiences significant local shear strain and is removed from the parent materials to generate chips [46].

The formation of such DTL features is normally attributed [45] to the upwards and downwards movement of dislocations with edge components perpendicular to the surface, as deformation is introduced, either by cutting or sliding wear. These dislocation components are then thought to collect at the DTL, to effectively form a low-angle grain boundary (i.e. a crystal defect-accommodated step change in crystal orientation across a certain area), with surprisingly high reported angles for this dislocation wall mechanism: up to 30° in pure copper [26], beyond which a further DTL is thought be required to accommodate further dislocations and the corresponding rotation. The presently observed HAB in Ni superalloy, at ~15°, complies with this; however the single HAB in Section 3.3, alone accommodating a rotation of ~45°, puts both this 30° angular limit, and the complete dislocation arrangement theory into question: it is not feasible to create a 45° boundary with a low-angle edge dislocation packing approach, the FCC ordinary dislocation cores are simply too close. The misorientation map (Area III in Fig. 6b) also indicates that the crystal rotation evolving into HAB and HDR is generated before the cut edge reaches this position. Undoubtedly, sub-region R6 is key to understanding the formation of the HAB; however, we do not yet have a complete picture of the mechanisms at play. It is clear that

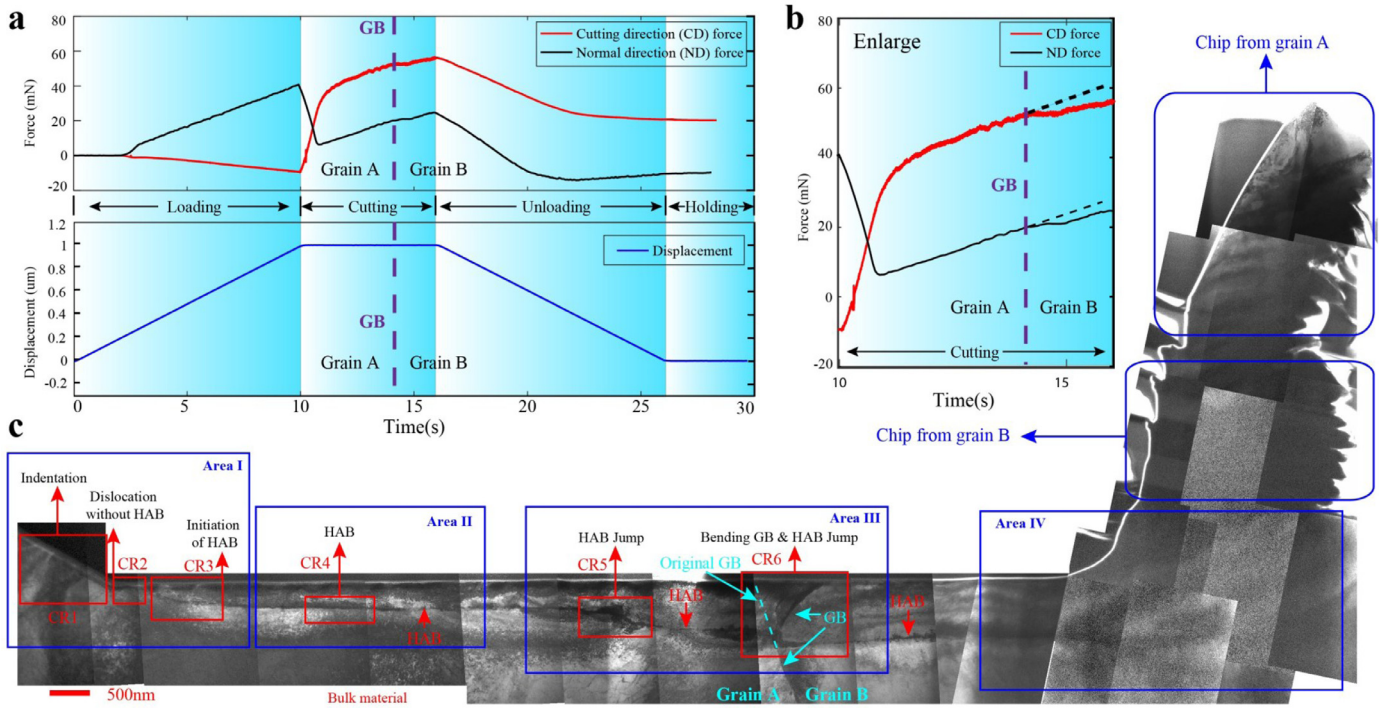

Fig. 7. Stitched bright field TEM images of the lamella lifted from the cross-GB cutting and the corresponding cutting forces. a, The cutting force variation and displacement of the tip during the cross-GB cutting. A constant cutting depth (1 μm) with 12 μm length cut reveals a force distortions in both normal and cutting directions when the tip approaches and crosses the GB areas. (Note: force this level of force variation has been found in every cross GB cutting, which means that this is the influence by GB rather than signal noise). **b**, Enlarged view of force variation when the tip approaches the GB and the transitory constant stage (horizontal level without increasing) just after crossing the GB. **c**, An overview TEM image of the cross-GB cutting lamella, showing the deformation layer and formation of different shape of the chips for grains A and B. Different cutting areas (i.e. initial indentation, single grain, cross-grain and material pile-up) are annotated. Area I and II are similar to the former single grain lamella sample; clear HAB steps, associated with a GB bending, are observed in Area III when approaching and upon crossing the GB. Clearly different chip morphology for grains A and B can be found, which correlate to the different grain orientations and the force variation.

mobile dislocations with non-zero momentum components in the ND direction exist (slip traces in HDR), as current thinking would require, yet the exact nature of the HAB remains elusive: further analysis is required to understand how accumulation of dislocations at a plane can lead to an abrupt lattice rotation anywhere between 7° and 45°, to state only the currently reported DTL rotation range. Either way, it is clear that the modified surface of the grain shows that the deformation depth (HAB) and influenced layers (HDR) do not simply depend on the classical shear phenomenon at the base of the material pile-up, or on the local tool edge radius ploughing, because the HAB starts to appear ahead of the tool edge in the area deep below the pile-up (detail of R6 given in Supplementary Explanation SE3).

The change in depth of this horizontal boundary feature as cutting progress, Fig. 6a, also requires further consideration, and to be related to the evolution (left to right) from a region of dislocation-mediated progressive lattice rotation at the initial indent, into an abrupt, high misorientation angle interface. As mentioned, the cutting and normal forces increase with growing material pile-up (linear increase in volume) in front of the cutting tip. In the tribological DTL theory, the stress state, particularly normal to the surface, is considered dominant in determining the DTL depth: crystal orientation effects in FCC metals are simply overcome by the high number of slip systems [26]. This premise will, however, be put into question in Section 3.3. Nevertheless, in this single crystal example, the increasing normal force indeed agrees with the theory of hence deeper penetration of dislocations with components parallel to ND, which eventually form the HAB at increasing depths.

To understand the character of the horizontal boundary feature as cutting progress, one must consider size effects in the generation of plasticity-mediating dislocations as cutting progress for such nanoscale depths of deformation. Indeed, initially, the volume solicited for deformation is relatively small, extending less than 200 nm deep, Fig. 6a, as a result of a low cutting force and little to no pile-up occurring (R2), and so few dislocations are initially present in this volume: their nucleation likely occurs in avalanches at the contact surface with the tip, similarly to nucleation-limited starvation regimes in other small-scale studies on metals [47]. As forces and deformation depths increase, the movement of a larger number of pre-existing dislocations in the correspondingly larger volume is incited, and eventually nucleation within the material volumes well ahead of the tip certainly occurs, as is evidenced in sub-region R6. Even then, due to the persisting effect of small length scales, the flow stress is expected to remain higher than in the macroscale regime.

In summary, the deformation behaviour in the near-surface region of a single grain at micro/nano-cutting scales is dominated by different mechanisms than the simplifications of classical cutting theory evoke. The cutting-induced crystal lattice rotation is limited to the CD-ND plane, while the highly dislocated region (HDR) is separated from the bulk of the grain by a gradually formed HAB. These results hint that the current understanding of single grain deformation behaviours in the shear-based material removal scenario, and the corresponding theory for micro/nano cutting simulation, may need to be seriously reconsidered [1,31,41].

3.3. Cross-Grain boundary cutting

Recognising that in the nano-cutting regime the deformation mechanisms diverge from the classical theory, and considering that grain boundary structures are known to play a significant role in the mechanical performance of polycrystalline materials [19], it is

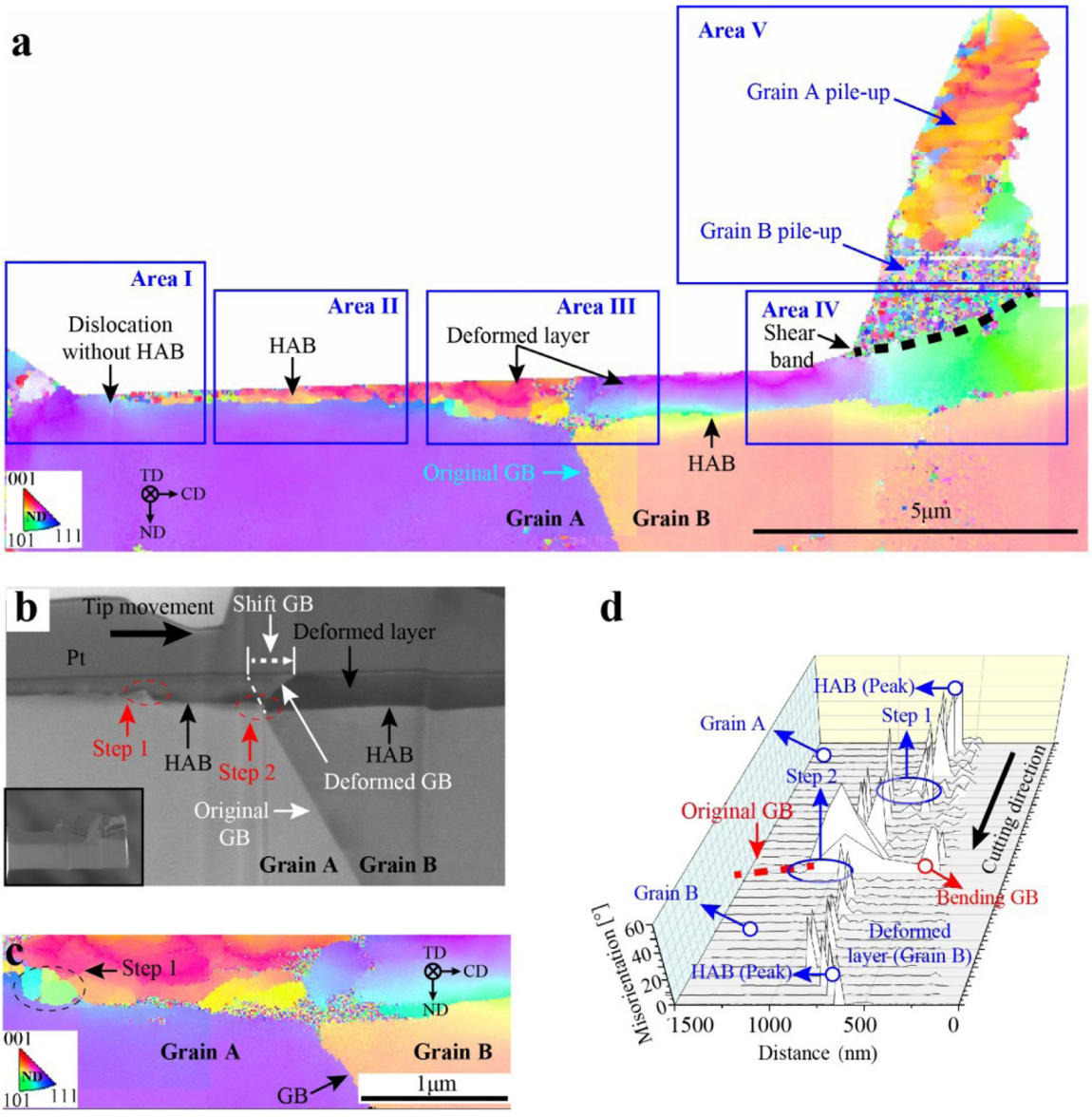

Fig. 8. Nano-cutting crossing and the investigation of GB deformation and subsurface misorientation caused by material removal. a, TKD map (IPF||ND) of the lift-out lamellar when nano-cutting crossing a GB. The deformation difference on each side of the GB presents the crystal rotation under loading; the initial cutting area shows dislocations without HAB and, with sufficient dislocation accumulation, the HAB is generated. Area I: simple lattice bending and the HAB initiation stage. Area II: the mid-cut part where a steady HAB has been formed. Area III: the GB area after nano-cutting which presents the GB bending and HAB jumps. Area IV and Area V are where the deformation of the existing near-surface layer is initiated as a result of loading by the cutting tip, and it includes the HAB formation, shear bands and the material pile-up. b, An ion contrast channelling image of the enlarged GB areas after nano-cutting revealing the GB being shifted (bent) and generated HAB jump when approaching and crossing the GB. c, Higher resolution TKD map of the enlarged GB area relative to the sample surface normal (IPF||ND); a clear grain recrystallization is found in the step 1 area where the HAB depth increased significantly. d, Point–to-point misorientation peak of the enlarged GB areas after the material removal, showing a HAB with ~45° angle and the HAB depth variation.

worthwhile to investigate the subsurface deformation (e.g. lattice rotation) caused by the cutting tip crossing grain boundaries (see overview image of cross-GB cut lift-out in Supplementary Explanation SE4-(1)). The GB studied in this case study is a Σ3 coherent twin boundary.

Comparing this with nano-cutting of single grains, measurements of both the cutting forces and the morphology of material pile-up (Fig. 7a), display clear changes when the cutting edge crosses the GB, where the normal and cutting direction forces present a step reduction (Fig. 7b) but the overall trend of increasing forces with pile-up volume are nevertheless maintained within each grain. Dissimilar chip morphologies (Fig. 3b; as well as in Fig. 7) are generated for grains A and B when crossing the GB, in contrast to the smooth single grain cutting case (Figs. 6a and3a). In this cutting for a crossing GB scenario, the upper part of the chip (formed from Grain A) is thinner than the lower part (formed from Grain B), while there is a clear separation between these parts (Fig. 3b; as well as in Fig. 7). These give an indication that the response of the grains to cutting load depends on their orientation relative to the cutting direction, and that the influence of the GB is not negligible in determining the deformation behaviour upon material removal processes. It is worth to note that the deformed layer in grain B is not increasing gradually in thickness from zero. This is because when the cutting tip initially interacts with grain A, the growing material pile-up (i.e. chip) increases the reaction (cutting) forces which, in turn, generates stresses ahead of the cutting tip that, as cutting progresses, induce deformations into both the grain boundary as well as already into the follow-up grain (i.e. B).

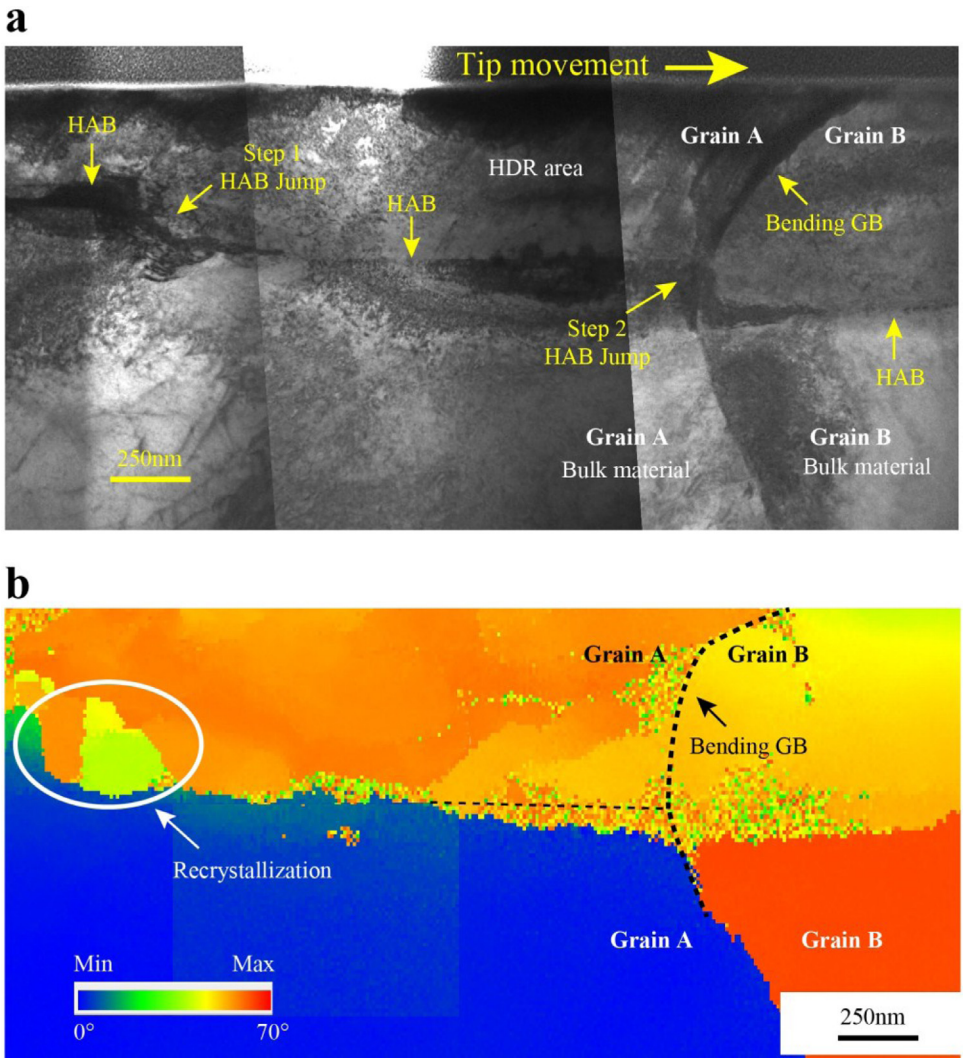

Fig. 9. Overview of across the GB zone revealing the nano-structure variation after nano-cutting. a, Transmission electron imaging (TEM) shows the non-deformed bulk and the deformed layer of both A and B grains as well as the GB areas. In the GB areas, clear GB bending is seen in the deformed layer because of the loading induced by the cutting tip while two steps in the HAB depth occur close to the GB. b, Two small recrystallized grains are found inside grain A at the position of step 1 in HAB depth.

The full TKD map upon nano-cutting across a GB (Fig. 8a) presents a significant variation in crystal orientation within the deformed layers of both grains *A* and *B* in comparison with their bulk structures. The difference in the crystal orientation between the deformed layer above each of grains A and B confirms that the initial orientation indeed affects the orientation of the final machined surface for a same nano-cutting condition. As for the previous single grain case, the misorientation map (Supplementary Explanation SE4-(2)) displays misorientation accumulation at the start of the cutting in grain A before HAB generation (Area I), and where cutting stops, a gradual variation in crystal orientation in the forward direction in the region between HAB and shear band (Area IV). Although these findings when nano-cutting across a GB (e.g. pile-up materials, shear bands, and HAB generation) display the same generic phenomena as those found in monocrystal nano-cutting (Fig. 6b), the existence of the original GB between grain A and B has brought an evident difference on the deformation mechanism of cutting-affected superficial layers at the GB zone (see Area III in Fig. 8), as well as on the material pile-up (see Area *V* in Fig. 8).

When focusing on the central region of the TEM lamella, Fig. 8b (detailed illustration, including the whole lamella, can be seen in Supplementary Explanation SE4-(1)), a clear deformation (bending) of the GB can be found, i.e. shift of the GB (around 500 nm) in the cutting direction at the newly exposed surface, compared with the original GB position; this draws a parallel with the finding for a tribological investigation on GB deformation [26]. With reference to the original position of the GB, the deformed layer of grain A caused by nano-cutting has crossed the original GB position and lies above the deformed layer of grain B, demonstrating the shift of the GB in the direction of cutting tip displacement. The clear HABs separating the HDR and bulk materials are identified in both grains A and B, similarly to the monocrystal case. However, the deformation depth in these two grains shows significant differences. The HAB inside grain A displays a clear step (step 1, Fig. 8b), indicating a sudden increase of the deformation depth, while another step of deformation depth (step 2, Fig. 8b) appears in the GB zone evidencing a different deformation phenomenon between grains A and B either side of the boundary. This suggests the HAB in grain A approaches the GB and is potentially arrested until the local stress is sufficient for a new HAB to be activated in grain B, that is, once strain transfer across the GB eventually occurs (e.g. by dislocations transmission) [48,49]. It is worth noting that this phenomenon occurring in the present nano-cutting differs from a case study in tribological loading [26] where no change in HAB depth was observed when crossing a twin boundary. It is again true that reciprocating normal loads of hundreds or thousands of cycles pro-

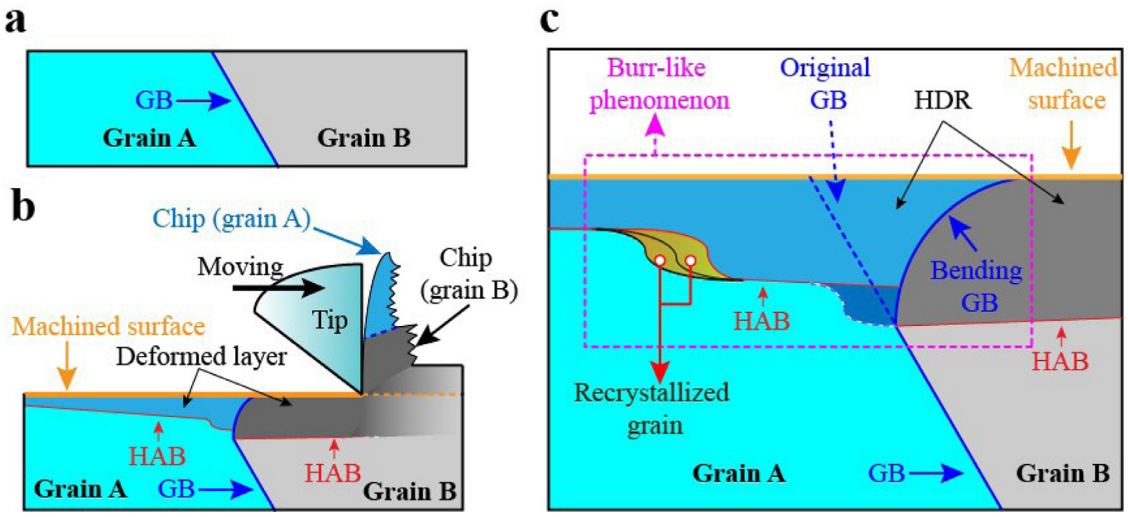

Fig. 10. The burr-like phenomenon in near-surface areas at cross-GB cutting. a, Original state and relative position of GB, grain A and grain B. **b**, Illustration of deformed near-surface layer (HDR area), bending GB, generated HAB trajectory and formed chips after cutting tip crosses the GB. **c**, Enlarged view at the GB crossing areas. The GB bending during nano-cutting could be considered similar to a burr generation phenomenon when cutting metals at macroscale. The different extents of dislocation accumulation that leads to the HAB step is similar to that expected as a result of the stress distribution causing burr generation, while the stress accumulation in the present study not only changes the HAB trajectory, but also causes grain recrystallisation (refer to Fig. 9b). The burr-like deformation of grain A, and resulting bending of the GB, emphasise the importance of considering the existence of GBs and the relative 'softness' of grains when studying the effect of cutting on the subsurface nanostructure of polycrystalline materials.

duce a different stress state than the intensive, short-lived loading of cutting. However, the fact that it is seen here that initial grain orientation can affect both the force of cutting and the HAB depth, as shall be discussed further below, suggests more extensive investigations into grain orientation effects on the tribological DTL could also be meritorious.

In the higher resolution TKD measurement of the enlarged GB zone – Area III (Fig. 8c), an interesting observation is worth emphasising: recrystallization appears inside grain A in the HAB jump position (Step 1 zone in Fig. 8c) as a result of the mechanical loading. This indicates that the material in the HAB jump zone has experienced significant dislocation accumulation, thus leading to grain nucleation to reduce the local dislocation density. The newly generated Σ3 twinned 400 nm diameter grain with low internal misorientation possesses a very different orientation compared with the surrounding HDR areas generated by gradients of lattice rotation, suggesting a random orientation of nucleation.

Regarding the point-to-point misorientation peaks (Fig. 8d) of enlarged Area III (whole lamellar area is presented in Supplementary Explanation SE4-(2)), the formed HAB in both grains A and B shows a misorientation value up to ~45° While normally the lattice rotation induced grain boundary is considered of the order of 15° in the constraint-free condition [50], the observed HAB (~ 45°) caused by nano-cutting is thought to result from the rotation being limited by the surrounding material, thus leading to the appearance of over-range rotation angles, see further analysis later. Of course, the rotation angles also depend on the original grain orientation; in comparison, the nano-cutting of the specific single grain (monocrystal) case above generated a HAB near to 15° (Fig. 5d).

TEM imaging (Fig. 9) of the region confirms the previous observations, in terms of the positions of twin and HAB boundaries. Furthermore, slip traces within the HDR above grain A, oriented at ~55° to the CD direction, evidence plasticity with a non-zero component in the cutting direction. In this, the ~70° 'bent' twin boundary is crucial, that is to say it is not simply a reoriented plane, but rather curved towards the pile-up material. Indeed, assuming that all deformation is accommodated elastically and by dislocation motion, the grain boundary movement must be mediated by dislocation with components of the simple cutting shear type (in CD direction). And in that, a higher number of dislocations must have impinged the boundary at a shallow depth, than closer to the HAB, in order to generate the differences in cumulative Burgers vectors with depth that lead to the grain boundary curvature. The coherent Σ3 twin boundary itself is not thought to pose much resistance to dislocation transfer [51]. This plasticity gradient may well be physical evidence of the stress gradients ahead of and below the cutting tool.

The bending of the GB shows a similar phenomenon to burr formation in macro cutting [52,53], whereby the stress field ahead of the tool dives into the material depth as a lesser resistance medium is approached due to the absence of reactive force, such as at the edge of a workpiece. In this case, the force drop (Fig. 7) at the GB zone suggests that grain B is relatively easier to deform ("softer") than grain A in this given cutting geometry: there is less mechanical resistance to cutting in the area to the right of the original GB when the deformation approaches the GB. And indeed the deformation of grain A and the corresponding GB impinges into the volume of grain B upon nano-cutting. Additional comments are given in Supplementary Explanation SE5 and Fig. 10. Thus, by analogy with burr formation, we suggest that HAB step 1 occurs just prior to the initial impingement of grain A into the volume of grain B, as the tool stress field sinks deeper into the material. Such heightened deformation at the original HAB depth is consistent with the recrystallization of a new grain (Figs. 8c and9b), due to an increased dislocation density near the HAB that surpasses the energetic threshold for recrystallization. It is therefore unclear whether the deeper HAB position in grain B is directly a result of further sinking of the tool stress field by this burr-analogous mechanism, or rather a characteristic of the initial grain B crystal orientation; likely the concepts are related.

Such features reveal much about the fragile stability of the HAB. To form, sufficient dislocation accumulation is required, as seen in the single grain case (Area I in Fig. 6b). The step change in crystal orientation at the HAB must represent a kinetic or energetic benefit over the alternative of progressive lattice rotation across the HDR. The position of the HAB in a first grain is presumably dic-

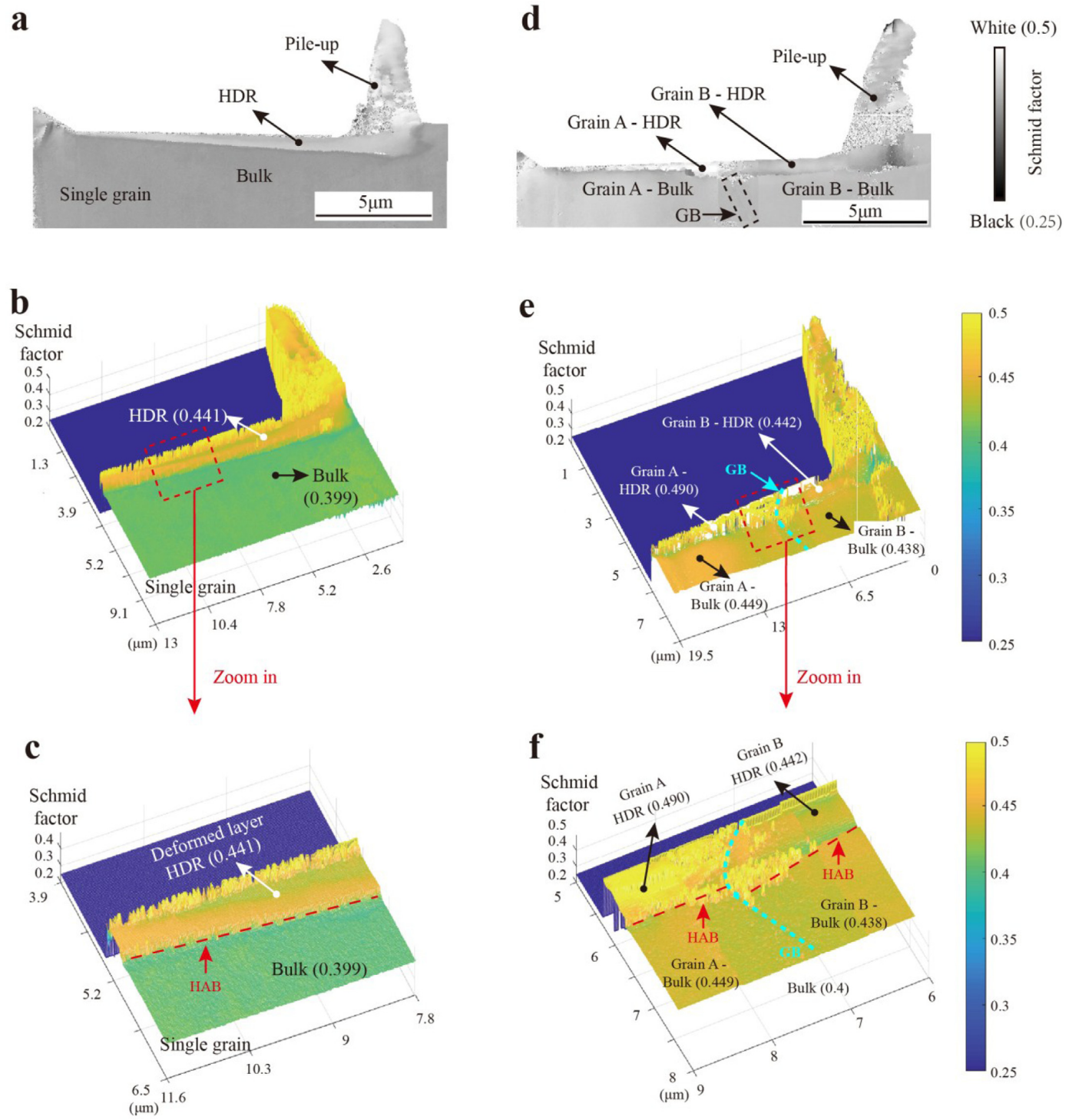

Fig. 11. Example of Schmid Factor (SF) distribution evaluated relative to the cutting direction on a monocrystal and cross-GB cutting. a, Overview of SF after single cutting that reveals different values between the deformed area (HDR) and bulk materials. **b**, 3-D view of the same SF. **c**, Enlarged area of **b** presenting the SF in the deformed area and the cliff (SF increasing edge) which corresponds to the previously observed HAB. **d**, Overview of the SF after crossing GB cutting which reveals SF difference. **e**, 3-D view of SF shows the previously commented variation, and the almost unchanged value in the deformed area of grain B. **f**, Enlarged area presents the SF in the deformed area and the cliff (SF increasing edge) at the GB area.

tated by the instantaneous local stress field at and ahead of the tool tip as it passes that location by. Whilst the HAB may exist stably in a single grain, microstructural barriers again put its existence into question, such as in the vicinity of a cut GB, where locally increased dislocation densities along the HAB are apparently of sufficient potential energy to cause recrystallization, with child grains replacing the HAB.

3.4. *Preferential* re-*orientation of cutting loaded crystals*

As is well known, the plastic deformation of crystalline materials depends on the shear stress applied on the slip plane and direction; thus, the materials undergoing shear-based operations (e.g. cutting) layers can be characterised by employing the geometric indicator of the Schmid factor to analyse the rotation of the crystal

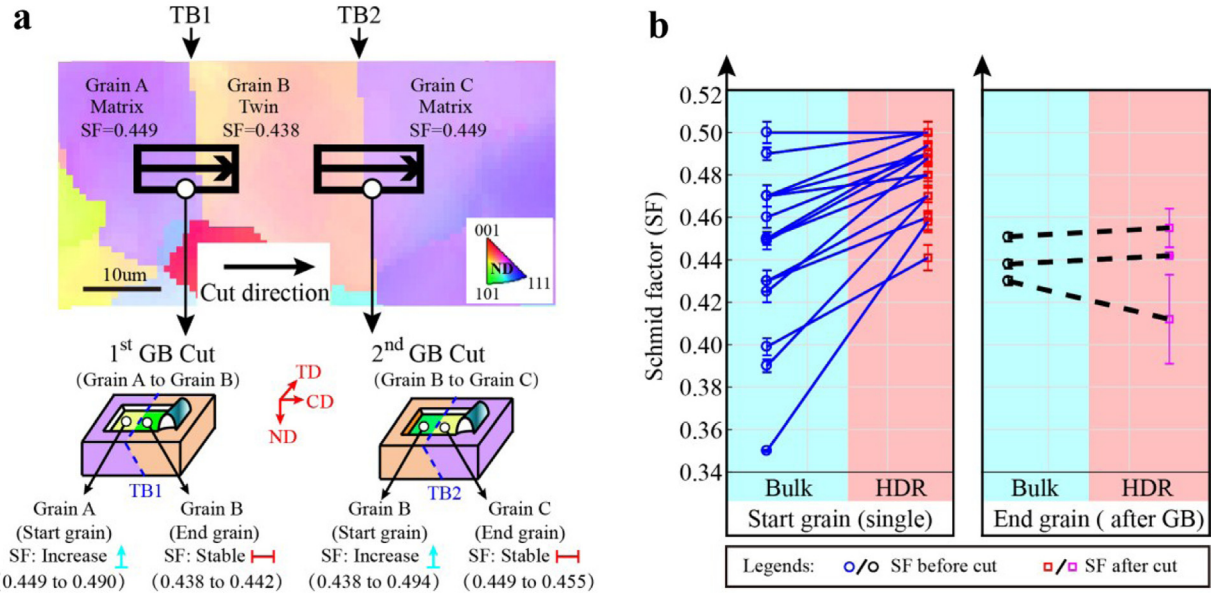

Fig. 12. Schmid factor variation before and after nano-cutting of both single and multiple grains. a, Illustration of two individual cuts, from (start) grain A to (end) grain B and from (start) grain B to (end) grain C, crossing two grain boundaries (GB1 and GB2) and the corresponding variations of the Schmid factor (SF) at the cut surface evaluated relative to the cutting direction (CD). For both cuts, the SF in the start grains has significantly increased but it does not vary significantly for the end grains. b, Statistical evaluation of SF variation before and after cutting for both start/single grains and end grains (after crossing GB). The SF at the surface after cutting in the start (or single) grain has significantly increased, while the end grain does not follow this trend, showing no significant variation.

lattice upon nano-cutting. It is well known that the stress state below a cutting tool tip is triaxial and complex, even with a neutral rake angle. As a step towards a first understanding of the mechanisms at play, the Schmid factor (SF) here is determined relative to the cutting force direction (CD), as this sees a significant increase in value during cutting (see Fig. 2a).

As an example of the many nano-cuts performed in this study, in the monocrystal cutting above, a clear increase of the average Schmid Factor of about 10% between the bulk of the grain and the deformed layer after cutting has been observed (see Fig. 11b where SF of 0.399 for the bulk of the grain compared with 0.441 for deformed layer); note that the increase of SF between the two zones was consistent throughout all the measured 15 points along the whole cutting length (detailed explanation can be found in Supplementary Explanation SE6). As an example of cross-GB cutting (Fig. 11d), interestingly, the SF in the deformed area (0.442) of grain B keeps almost the same value relative to the bulk (0.438), which differs to the tendency in grain A and monocrystal cases.

Furthermore, for cross-GB cutting (Fig. 12a) we present here an example of cutting three grains (A, B, C) with two respective twin boundaries (i.e. TB1 and TB2); the initial crystal orientations of grains A and C are identical. Considering the 1st GB cut from grain A (start grain) to grain B (end grain), a similar increase (ca. 9%) of SF in grain A has been observed (from 0.449 in bulk to 0.490 in deformed layer). However, after crossing the TB1, the deformed layer in grain B shows an insignificant increase of SF (0.438 for the bulk grain and 0.442 for the deformed layer). Thus, it could be considered that while the grain A (start grain) has the possibility to rotate to an easier deformation direction (represented by a higher SF), the deformation orientation in grain B (end grain) when the cutting tip crosses TB1 is defined by the deformation in grain A (start grain) and the bending of the GB; this means that the deformation in grain B needs to follow the direction imposed in the grain A which does not necessarily lead to significant SF increase in the second grain. Now, taking into account the 2nd GB cut (Fig. 12a), from the grain B (now considered as the start grain) to grain *C* (end grain) while crossing the nearby symmetrical TB2, it shows that the SF in grain B (start grain) after cutting increases from 0.438 to 0.494, and the SF in the grain *C* (end grain) presents a change from 0.449 to 0.455 (i.e. constant if considering measurement errors). This indicates that the second (end) grain (i.e. grain *B* in 1st cut and grain C in 2nd cut) could be considered unaffected by the cutting action, from the viewpoint of the Schmid factor in the CD direction (it is important to note that this does not mean that no crystal rotation occurs in the second grain, certainly much is measured, Fig. 9(b) – rather this rotation does not occur either in a direction, or to an extent, that results in a consistently increased SF relative to the CD direction). However, the first (start) grain (i.e. *A* grain in 1st cut and B grain in 2nd cut) increases significantly its SF (close to maximum SF = 0.5 – see follow-up discussions), and the grain rotation is large (ca. 45°) to achieve this. Much larger angles of rotation are measured than would normally be necessary to align with the nearest maximum SF orientation if the grain can rotate freely. This is specifically the point: we know from our measurements that the cutting restricts the grain from rotating around the most convenient axis; they are observed more to 'roll' within the x-y (cutting) plane along the cutting tip direction. So, they must rotate by a large angle until the Schmid factor is maximised. The divergent behaviour of grains *A* (=*C*), and *B*, depending on whether they are the first or second cut grains, leads to the conclusion that the extent of deformation in diverse grains in cross-GB cutting is significantly different from single grain cutting, which raises the necessity of serious consideration of material deformation mechanisms in the micro/*nano*-cutting of polycrystalline materials.

To statistically support the grain deformation principles we are putting forward, many more nano-cuts (over 20 in total, in 15 distinct single/start grains) were carried out on the same sample but on grains with different orientations, while the values of SF relative to the cutting direction have been evaluated before and after cutting (Fig. 12b). For all of the cuts in a single or first grain, the SF has consistently increased after cutting compared with the original bulk of grains although the extent of the increase depends on the original grain orientation. According to a paired *t*-test, the measured increase in the SF after cutting for the single or first (start) grains is statistically significant with a p value of 1.5×10^{-4} (note:

a p-value less than 0.05 is statistically significant). As known, a higher Schmid Factor (SF) represents a smaller external yield stress along that axis, indicating that the deformed material has a tendency to rotate to a "softer" crystal orientation relative to the cutting direction. This gives the possibility to predict the material's deformation tendency: it rotates in preference of a higher Schmid factor, which may be determined by knowing the loading direction and original crystal orientation; this is, therefore, especially applicable for the single crystal cutting applications. When considering the multiple grain cutting case (crossing GBs), the deformation of the subsequent/end grains does not share the trend of the single grain of an increasing SF: crystal rotation within the second (end) grain is controlled by considering the SF and deformation induced in the previously (first) cut grain and the corresponding GB geometry.

The present study cannot explain the specific reason for the first grains rotating towards a high Schmid factor in the CD direction upon being cut; further, more detailed, simulations of the tool tip stress field are required that are beyond the scope of this work. Nevertheless, much as Haug et al. [26] evoke, but for differing reasons (see Section 3.3), it is clear that the optimised crystal orientation of the HDR layer of such grains is far from the simplistic {111} $\perp$ ND, ⟨110⟩ || CD that would fulfil a simple in-plane (CD-TD) cutting shear; instead, slip planes inclined to both ND and CD (~30° and ~55° to CD in the case studies here) are preferred.

4. Conclusion

Finally, considering all the deformation phenomena of the superficial layers for both single grain and cross-GB nano-cutting, one may comment that this is quite different from the classic shear-plane theory generally accepted at the micro/*meso*/macro scales. As presented here, a variable dislocation extent (density and/or location) will be generated in a progressive manner following the evolution of cutting along a single grain, which contradicts the current knowledge that specific constant cutting parameters leads to constant deformation depth. We also found the lattice rotation in deformed layers is limited (in this cutting geometry) to a two-dimensional orthogonal plane defined by the cutting and normal directions; this highly dislocated region is clearly separated from the bulk of the grain by a generated high angle boundary (HAB). It is noted that the HAB progression is intimately related to the material pile-up in front of the cutting tip, emphasizing the importance of considering the influence of pile-up materials and the diverse deformation mechanisms in inter-grain scale shearing.

In particular, the cross-GB cutting investigations clearly present the influence of GBs on the deformation behaviour where multiple grains exist. We have observed that the monotonic increase of HAB depth is disrupted when the nano-cutting passed from one grain to another, a phenomenon that alters dislocation distributions in the near-GB region, leading to local recrystallization and influencing the deformation behaviour of the grains cut after the GB. In addition, the statistical investigation of the deformed layer over many tens of cuts revealed that the grains have a tendency to deform with a crystal rotation towards a softer orientation relative to the cutting direction. This suggests that the crystalline material presents a predictable deformation/rotation behaviour under a shear-based material removal process at the micro-to-nano scales.

These findings highlight the importance of this work in understanding the material deformation phenomena under micro/nano-cutting conditions, with many new considerations raised. For example, one may consider choosing a preferential in-plane (cutting) load direction to have less sub-surface deformation and a smaller reaction force for a given crystal orientation of a grain. Similarly, grain boundaries play non-negligible roles in micro/nano-cutting by influencing the deformation mechanism of the material (e.g. GB bending, or dislocation accumulation resulting in local recrystallization and HAB steps). It is also important to note that the cutting tip edge radius plays significant roles for the micro/nanoscale cutting mechanism and with its increase the reaction forces and the subsequent grain deformations associated with the material shearing is to increase as well; hence, the material deformation phenomena, commented in this work, that occur at grain level could change in magnitude and complexity. By considering the newly-observed deformation mechanisms in nano-cutting of single and multiple grains, this research has also a high potential to help the progress of state-of-art simulation work by strain gradient crystal plasticity simulation, validating modelling assumptions, and thus leading to accurate prediction of the material deformation under micro/nano and larger scale cutting.

Funding source

This work was supported by the Machining and Condition Monitoring Research Group from The University of Nottingham, Mechanics of Materials and Nanostructures group from Swiss Federal Laboratories for Materials Science and Technology (EMPA), MARIE SKŁODOWSKA-CURIE ACTIONS (H2020-MSCA-COFUND-2014): The Integration of Novel Aerospace Technologies "INNOVATIVE" (No: 665468) Marie Skłodowska-Curie grant agreement number 754364, and NanoPrime funding from the EPSRC (No: EP/R025282/1). T.E.J.E. received funding from EMPAPOSTDOCS-II of the European Union's Horizon 2020 research and innovation programme under the Marie Skłodowska-Curie grant agreement number 754,364.

Declaration of Competing Interest

The authors declare no competing interests.

CRediT authorship contribution statement

Dongdong Xu: Investigation, Formal analysis, Writing - review & editing. **Thomas E.J. Edwards:** Investigation, Formal analysis, Writing - review & editing. **Zhirong Liao:** Investigation, Formal analysis, Writing - review & editing. **Xavier Maeder:** Investigation, Formal analysis, Writing - review & editing. **Rajaprakash Ramachandramoorthy:** Investigation, Writing - review & editing, Formal analysis. **Manish Jain:** Investigation, Writing - review & editing. **Johann Michler:** Writing - review & editing, Formal analysis. **Dragos Axinte:** Formal analysis, Writing - review & editing, Conceptualization.

Acknowledgement

We thank Dr. Christopher Parmenter and Dr. Nigel Neate from the Nanoscale and Microscale Research Centre, University of Nottingham, for their support during FIB training (including marks fabrication and lamella preparation), and TKD and TEM measurement.

Supplementary materials

Supplementary material associated with this article can be found, in the online version, at doi:10.1016/j.actamat.2021.116929.

References

[1] F. Xu, F. Fang, Y. Zhu, X. Zhang, Study on crystallographic orientation effect on surface generation of aluminum in nano-cutting, Nanoscale Res. Lett. (2017) 12, doi:10.1186/s11671-017-1990-3.

[2] Z. Wang, J. Zhang, Z. Xu, J. Zhang, G. Li, H. Zhang, Z. Li, H. ul Hassan, F. Fang, A. Hartmaier, Y. Yan, T. Sun, Crystal anisotropy-dependent shear angle variation in orthogonal cutting of single crystalline copper, Precis. Eng. 63 (2020) 41–48, doi:10.1016/j.precisioneng.2020.01.006.

[3] Y. Ayed, C. Robert, G. Germain, A. Ammar, Orthogonal micro-cutting modeling of the Ti17 titanium alloy using the crystal plasticity theory, Finite Elem. Anal. Des. 137 (2017) 43–55, doi:10.1016/j.finel.2017.08.002.

[4] M. Jo, Y.M. Koo, B.J. Lee, B. Johansson, L. Vitos, S.K. Kwon, Theory for plasticity of face-centered cubic metals, Proc. Natl. Acad. Sci. U. S. A. 111 (2014) 6560–6565, doi:10.1073/pnas.1400786111.

[5] W. Huang, J. Yan, Surface formation mechanism in ultraprecision diamond turning of coarse-grained polycrystalline ZnSe, Int. J. Mach. Tools Manuf. 153 (2020) 103554.

[6] P.M. Anderson, J.P. Hirth, J. Lothe, Theory of Dislocations, Cambridge University Press, 2017.

[7] M.F. Chisholm, S. Kumar, P. Hazzledine, Dislocations in complex materials, Science 307 (2005) 701–703 (80-.).

[8] H. Van Swygenhoven, Grain boundaries and dislocations, Science 296 (2002) 66–67 (80-.).

[9] L. Margulies, G. Winther, H.F. Poulsen, In situ measurement of grain rotation during deformation of polycrystals, Science 291 (2001) 2392–2394 (80-.).

[10] U.F. Kocks, C.N. Tomé, H.-.R. Wenk, Texture and Anisotropy: Preferred Orientations in Polycrystals and Their Effect On Materials Properties, Cambridge university press, 1998.

[11] J.A. Wert, X. Huang, G. Winther, W. Pantleon, H.F. Poulsen, Revealing deformation microstructures, Mater. Today 10 (2007) 24–32.

[12] Y. Wang, M. Chen, F. Zhou, E. Ma, High tensile ductility in a nanostructured metal, Nature 419 (2002) 912–915.

[13] B. Jakobsen, H.F. Poulsen, U. Lienert, J. Almer, S.D. Shastri, H.O. Sørensen, C. Gundlach, W. Pantleon, Formation and subdivision of deformation structures during plastic deformation, Science 312 (2006) 889–892 (80-.).

[14] J. Wang, Z. Zeng, C.R. Weinberger, Z. Zhang, T. Zhu, S.X. Mao, *In situ* atomic-scale observation of twinning-dominated deformation in nanoscale body-centred cubic tungsten, Nat. Mater. 14 (2015) 594–600, doi:10.1038/nmat4228.

[15] S.H. Oh, M. Legros, D. Kiener, G. Dehm, *In situ* observation of dislocation nucleation and escape in a submicrometre aluminium single crystal, Nat. Mater. 8 (2009) 95–100, doi:10.1038/nmat2370.

[16] B. Regan, A. Aghajamali, J. Froech, T.T. Tran, J. Scott, J. Bishop, I. Suarez-Martinez, Y. Liu, J.M. Cairney, N.A. Marks, M. Toth, I. Aharonovich, Plastic deformation of single-crystal diamond nanopillars, Adv. Mater. 32 (2020) 1–7, doi:10.1002/adma.201906458.

[17] N.K. Bourne, Materials science: atomistic views of deformation, Nature 550 (2017) 461–463.

[18] C.J. Youngdahl, J.R. Weertman, R.C. Hugo, H.H. Kung, Deformation behavior in nanocrystalline copper, Scr. Mater. 44 (2001) 1475–1478.

[19] L.H. Van Vlack, Elements of Materials Science and Engineering, Addison-Wesley New York, 1985.

[20] Z.C. Lin, J.C. Huang, Y.R. Jeng, 3D nano-scale cutting model for nickel material, J. Mater. Process. Technol. 192–193 (2007) 27–36, doi:10.1016/j.jmatprotec.2007.04.074.

[21] C. Li, Q. Zhang, Y. Zhang, F. Zhang, X. Wang, G. Dong, Nanoindentation and nanoscratch tests of YAG single crystals: an investigation into mechanical properties, surface formation characteristic, and theoretical model of edge-breaking size, Ceram. Int. 46 (2020) 3382–3393, doi:10.1016/j.ceramint.2019.10.048.

[22] S. Sawamura, R. Limbach, H. Behrens, L. Wondraczek, Lateral deformation and defect resistance of compacted silica glass: quantification of the scratching hardness of brittle glasses, J. Non Cryst. Solids 481 (2018) 503–511, doi:10.1016/j.jnoncrysol.2017.11.035.

[23] B. Meng, Y. Zhang, F. Zhang, Material removal mechanism of 6H-SiC studied by nano-scratching with Berkovich indenter, Appl. Phys. A Mater. Sci. Process. 122 (2016) 1–9, doi:10.1007/s00339-016-9802-7.

[24] Y. He, L. Zhong, F. Fan, C. Wang, T. Zhu, S.X. Mao, *In situ* observation of shear-driven amorphization in silicon crystals, Nat. Nanotechnol. 11 (2016) 866–871, doi:10.1038/nnano.2016.166.

[25] J.G. Gigax, J.K. Baldwin, C.J. Sheehan, S.A. Maloy, N. Li, Microscale shear specimens for evaluating the shear deformation in single-crystal and nanocrystalline Cu and at Cu-Si interfaces, J. Mater. Res. 34 (2019) 1574–1583, doi:10.1557/jmr.2019.104.

[26] C. Haug, F. Ruebeling, A. Kashiwar, P. Gumbsch, C. Kübel, C. Greiner, Early deformation mechanisms in the shear affected region underneath a copper sliding contact, Nat. Commun. (2020) 11, doi:10.1038/s41467-020-14640-2.

[27] V. Yamakov, D. Wolf, S.R. Phillpot, A.K. Mukherjee, H. Gleiter, Dislocation processes in the deformation of nanocrystalline aluminium by molecular-dynamics simulation, Nat. Mater. 1 (2002) 45–48, doi:10.1038/nmat700.

[28] S.J. Zhou, D.L. Preston, P.S. Lomdahl, D.M. Beazley, Large-scale molecular dynamics simulations of dislocation intersection in copper, Science 279 (1998) 1525–1527 (80-.).

[29] S. Goel, X. Luo, A. Agrawal, R.L. Reuben, Diamond machining of silicon: a review of advances in molecular dynamics simulation, Int. J. Mach. Tools Manuf. 88 (2015) 131–164, doi:10.1016/j.ijmachtools.2014.09.013.

[30] V. Bulatov, F.F. Abraham, L. Kubin, B. Devincre, S. Yip, Connecting atomistic and mesoscale simulations of crystal plasticity, Nature 391 (1998) 669–672.

[31] K.S. Djaka, A. Moufki, M. Nouari, P. Laheurte, A. Tidu, A semi-analytical modelling of cutting using crystal plasticity theory and flow line approach, Int. J. Mech. Sci. 146–147 (2018) 49–59, doi:10.1016/j.ijmecsci.2018.07.034.

[32] S.A. Tajalli, M.R. Movahhedy, J. Akbari, Simulation of orthogonal micro-cutting of FCC materials based on rate-dependent crystal plasticity finite element model, Comput. Mater. Sci. 86 (2014) 79–87, doi:10.1016/j.commatsci.2014.01.016.

[33] Y. Zhang, T. Mabrouki, D. Nelias, C. Courbon, J. Rech, Y. Gong, Cutting simulation capabilities based on crystal plasticity theory and discrete cohesive elements, J. Mater. Process. Technol. 212 (2012) 936–953, doi:10.1016/j.jmatprotec.2011.12.001.

[34] R. Komanduri, N. Chandrasekaran, L.M. Raff, M.D. simulation of nanometric cutting of single crystal aluminum-effect of crystal orientation and direction of cutting, Wear 242 (2000) 60–88, doi:10.1016/S0043-1648(00)00389-6.

[35] X. Kong, P.H. Cohen, J. Dong, Predictive modeling of feature dimension for tip-based nano machining process, J. Manuf. Process. 24 (2016) 338–345, doi:10.1016/j.jmapro.2016.06.013.

[36] H. Luo, H. Sheng, H. Zhang, F. Wang, J. Fan, J. Du, J.Ping Liu, I. Szlufarska, Plasticity without dislocations in a polycrystalline intermetallic, Nat. Commun. 10 (2019) 1–8, doi:10.1038/s41467-019-11505-1.

[37] H. Ding, Y.C. Shin, Dislocation density-based grain refinement modeling of orthogonal cutting of titanium, J. Manuf. Sci. Eng. Trans. ASME 136 (2014) 1–11, doi:10.1115/1.4027207.

[38] J. Bai, Q. Bai, Z. Tong, Dislocation dynamics-based modeling and simulations of subsurface damages microstructure of orthogonal cutting of titanium alloy, Micromachines (Basel) 8 (2017) 309.

[39] D.V. Lychagin, S.Y. Tarasov, A.V. Chumaevskii, E.A. Alfyorova, Strain-induced folding on [1 1^{-} 1^{-}]-copper single crystals under uniaxial compression, Appl. Surf. Sci. 371 (2016) 547–561, doi:10.1016/j.apsusc.2016.02.232.

[40] J.B. Hannon, V.B. Shenoy, K.W. Schwarz, Anomalous spiral motion of steps near dislocations on silicon surfaces, Science 313 (2006) 1266–1269 (80-.).

[41] Z. Wang, J. Zhang, Z. Xu, J. Zhang, H. ul Hassan, G. Li, H. Zhang, A. Hartmaier, F. Fang, Y. Yan, T. Sun, Crystal plasticity finite element modeling and simulation of diamond cutting of polycrystalline copper, J. Manuf. Process. 38 (2019) 187–195, doi:10.1016/j.jmapro.2019.01.007.

[42] L. Nicola, A.F. Bower, K.S. Kim, A. Needleman, E. Van der Giessen, Surface versus bulk nucleation of dislocations during contact, J. Mech. Phys. Solids 55 (2007) 1120–1144, doi:10.1016/j.jmps.2006.12.005.

[43] X.L. Yuan, T. Sekiguchi, J. Niitsuma, Y. Sakuma, S. Ito, S.G. Ri, Inhomogeneous distribution of dislocations in a SiGe graded layer and its influence on surface morphology and misfit dislocations at the interface of strained $Si/Si_{0.8}$ $Ge_{0.2}$, Appl. Phys. Lett. 86 (2005) 162102.

[44] Z. Liao, M. Polyakov, O.G. Diaz, D. Axinte, G. Mohanty, X. Maeder, J. Michler, M. Hardy, Grain refinement mechanism of nickel-based superalloy by severe plastic deformation - mechanical machining case, Acta Mater. 180 (2019) 2–14, doi:10.1016/j.actamat.2019.08.059.

[45] C. Greiner, Z. Liu, R. Schneider, L. Pastewka, P. Gumbsch, The origin of surface microstructure evolution in sliding friction, Scr. Mater. 153 (2018) 63–67.

[46] M.C. Shaw, J.O. Cookson, Metal Cutting Principles, Oxford university press, New York, 2005.

[47] W.D. Nix, J.R. Greer, G. Feng, E.T. Lilleodden, Deformation at the nanometer and micrometer length scales: effects of strain gradients and dislocation starvation, Thin Solid Films 515 (2007) 3152–3157.

[48] Q. Ding, X. Fu, D. Chen, H. Bei, B. Gludovatz, J. Li, Z. Zhang, E.P. George, Q. Yu, T. Zhu, R.O. Ritchie, Real-time nanoscale observation of deformation mechanisms in CrCoNi-based medium- to high-entropy alloys at cryogenic temperatures, Mater. Today 25 (2019) 21–27, doi:10.1016/j.mattod.2019.03.001.

[49] F. Di Gioacchino, T.E.J. Edwards, G.N. Wells, W.J. Clegg, A new mechanism of strain transfer in polycrystals, Sci. Rep. 10 (2020) 1–15.

[50] L.A. Barrales-Mora, 2D and 3D Grain Growth Modeling and Simulation, Cuvillier Verlag, 2008.

[51] N.V. Malyar, J.-.S. Micha, G. Dehm, C. Kirchlechner, Dislocation-twin boundary interaction in small scale Cu bi-crystals loaded in different crystallographic directions, Acta Mater 129 (2017) 91–97.

[52] J.C. Aurich, D. Dornfeld, P.J. Arrazola, V. Franke, L. Leitz, S. Min, Burrs analysis, control and removal, CIRP Ann. 58 (2009) 519–542.

[53] M. Hashimura, J. Hassamontr, D.A. Dornfeld, Effect of in-plane exit angle and rake angles on burr height and thickness in face milling operation, J. Manuf. Sci. Eng. 121 (1999) 13–19.